Intrinsic ultralow lattice thermal conductivity of the unfilled skutterudite $FeSb_3$

Yuhao Fu,[1] David J. Singh,[3] Wu Li,[2,*] and Lijun Zhang[1,†]

[1]*College of Materials Science and Engineering and Key Laboratory of Automobile Materials of MOE, Jilin University, Changchun 130012, China*

[2]*Institute for Advanced Study, Shenzhen University, 3688 Nanhai Avenue, Shenzhen 518060, China*

[3]*Department of Physics and Astronomy, University of Missouri, Columbia, Missouri 65211-7010, USA*

(Received 22 March 2016; published 11 August 2016)

It is generally accepted that unfilled skutterudites process high lattice thermal conductivity κ_l that can be efficiently reduced upon filling. Here by using first-principles Boltzmann-Peierls transport calculations, we find pure skutterudite of $FeSb_3$ with no filler in fact has an intrinsic ultralow κ_l smaller than that of $CoSb_3$ by one order of magnitude. The value is even smaller than those of most of the fully filled skutterudites. This finding means that with $FeSb_3$ as a reference, filling does not necessarily lower κ_l. The ultralow κ_l of $FeSb_3$ is a consequence of the overall softening of phonon spectrum, especially the lowering in frequency of optical phonon branches associated with the weakly bonded Sb_4 rings. They overlap more with heat-carrying acoustic phonons and significantly increase the phase space for three-phonon anharmonic scattering processes. This provides an alternative non-filling-related mechanism for lowering the κ_l of skutterudites.

DOI: 10.1103/PhysRevB.94.075122

I. INTRODUCTION

Skutterudites are an important class of high-performance thermoelectrics [1–20] as the embodiment of Slack's "electron-crystal phonon-glass" idea [21]. The existence of two icosahedral voids in their crystal structures allows for filling in a variety of cations (e.g., rare earth, alkali earth, or alkali metals). This offers dual advantages for good thermoelectrics: first, according to the Zintl concept, the additional electrons transferred from the electropositive fillers to the $CoSb_3$ framework make possible flexible control of n-type doping [4,7,8,10,11,15–17,22,23] and provide compensating change to the p-type doping with Co replaced by electron-deficient Fe [1,2,5,8,14,24]. Second, and more importantly, filling strongly lowers lattice thermal conductivity κ_l [1–4,7,8,10,11,15,17–19,22], and optimizing the filling to lower κ_l both in terms of filling fraction and by using suitable mixtures of filled cations plays a central role in the optimization of high-performance skutterudite thermoelectrics [4].

The physical mechanism responsible for the reduction of κ_l in filled skutterudites remains elusive after two decades of intensive research. There are several debated aspects about the nature and role of the vibrations associated with the filled "rattling" atoms: (i) whether the motion of the rattling atoms is incoherent and noncorrelated [21,25–27] or coherently couples with the host framework [28,29], (ii) whether anharmonic interaction exists between the localized rattling modes and the propagating phonons of the host framework [30–34], and (iii) whether the reduction of κ_l originates from the energy dissipation caused by the resonant scattering of the rattling atoms [2,21,25,35] or the enhanced conventional anharmonic scattering processes [29,33,34,36].

Despite controversy over the mechanism, there is consensus that the filling should reduce κ_l of skutterudites. In this paper we report the finding via first-principles transport calculations that the recently reported skutterudite $FeSb_3$ [37–42] often presumed to be closely related to $CoSb_3$ in fact has a very low κ_l without filling, even lower than those of most of the fully filled skutterudites (e.g., with Ba, La, and Ce). This unexpected finding indicates that filling does not necessarily lower κ_l of skutterudites. The ultralow κ_l in the unfilled $FeSb_3$ skutterudite is a consequence of the overall softening of phonon spectrum, especially the lowering in frequency of optical phonon branches that take the role of the rattling modes in the filled skutterudites. The resultant optical-acoustic phonon overlapping increases three-phonon anharmonic scattering channels, thus significantly reducing phonon lifetimes and κ_l. Our result provides an alternative non-filling-related routine to realize low κ_l in skutterudites.

II. METHOD

We perform first-principles calculations of κ_l for $FeSb_3$ and fully filled skutterudites of $La/CeFe_4Sb_{12}$ by iteratively solving the linearized Boltzmann-Peierls transport equation of phonons with the SHENGBTE package [43]. The equilibrium crystal structures and interatomic force constants (IFCs) are obtained from density-functional theory (DFT) calculations with the plane-wave projector-augmented-wave method [44], as implemented in the VASP code [45]. We employ the local-density approximation (LDA) as an exchange-correlation functional. A ferromagnetic configuration for $FeSb_3$ is used which is the lowest-energy magnetic configuration at the LDA level. We did calculations with both LDA and generalized gradient approximation (GGA) functionals and found in both cases that ferromagnetic ordering is preferred over near-neighbor antiferromagnetic order. As noted in prior work by Råsander and coworkers [41], magnetism is important for the stability of this compound. Structural optimization is done with the kinetic-energy cutoffs of 350 eV or more and the $8 \times 8 \times 8$ k-point mesh, which ensures residual forces smaller than 1×10^{-4} eV/Å. The resulting equilibrium lattice constants are slightly smaller than the experimental data (by 2.03%, 1.78%, and 2.00% for $FeSb_3$, $LaFe_4Sb_{12}$,

*wu.li.phys2011@gmail.com

†lijun_zhang@jlu.edu.cn

 ©2016 American Physical Society

TABLE I. Optimized structure parameters by total energy minimization for $FeSb_3$, $CoSb_3$, $LaFe_4Sb_{12}$, and $CeFe_4Sb_{12}$ compared with available experimental data [12,24,37].

		Lattice parameter	Fractional coordinates	
		a	x	y
$FeSb_3$	Theory	8.968	0.329	0.161
	Expt.[a]	9.154	0.334	0.158
$CoSb_3$	Theory	8.918	0.332	0.160
	Expt.[b]	9.0345		
$LaFe_4Sb_{12}$	Theory	8.985	0.335	0.164
	Expt.[c]	9.148		
$CeFe_4Sb_{12}$	Theory	8.957	0.333	0.164
	Expt.[c]	9.140		

[a]Reference [37].
[b]Reference [12].
[c]Reference [24].

and $CeFe_4Sb_{12}$, respectively), as summarized in Table I. The agreements are reasonably good when considering the usual underestimation of lattice constants in the DFT-LDA calculations. The harmonic and third-order anharmonic IFCs are calculated by using the real-space supercell approach [43,46] in $3 \times 3 \times 3$ supercells with a $2 \times 2 \times 2$ k-point mesh and $2 \times 2 \times 2$ supercells with a $3 \times 3 \times 3$ k-point mesh, respectively. A phonon momenta q mesh of $15 \times 15 \times 15$ is used in solving the transport equation to ensure that κ_l converges at the 1×10^{-6} W/mK level.

By solving the linearized Boltzmann-Peierls transport equation of phonons, all the contributions from two-phonon and three-phonon scattering processes responsible for intrinsic κ_l of crystalline materials are included. Briefly, the isotopic κ_l of cubic skutterudites at temperature T can be represented as the sum of contributions over each phonon mode λ (with branch p and wave vector $\mathbf{q}$):

$$\kappa_l \equiv \kappa_l^{\alpha\alpha} = \frac{1}{NV}\sum_{\lambda} C_\lambda \upsilon_\lambda^\alpha \upsilon_\lambda^\alpha \tau_\lambda \tag{1}$$

and

$$C_\lambda = \frac{\partial f_\lambda(\omega_\lambda, T)}{\partial T}, \tag{2}$$

where N is the number of $\mathbf{q}$ points uniformly sampled in the phonon Brillouin zone, V is the unit-cell volume, C_λ is the phonon mode heat capacity, $f_\lambda(\omega_\lambda, T)$ is the Bose-Einstein distribution function, depending on the phonon angular frequency ω_λ and T, υ_λ^α is the phonon group velocity along the α direction, and τ_λ is the phonon lifetime. In bulk materials without impurities, τ_λ is determined by the processes of two-phonon scattering from isotopic disorder and three-phonon anharmonic scattering. In the relaxation-time approximation, τ_λ is equal to a sum of the isotope scattering rate $\frac{1}{\tau^{\rm iso}}$ and the anharmonic scattering rate $\frac{1}{\tau^{\rm anh}}$. For most of materials, $\frac{1}{\tau^{\rm iso}}$ is at least two orders smaller in magnitude than $\frac{1}{\tau^{\rm anh}}$. The anharmonic scattering rate $\frac{1}{\tau^{\rm anh}}$ can be calculated as the sum over λ of the three-phonon transition probabilities $\Gamma^{\pm}_{\lambda\lambda'\lambda''}$, which can be expressed as [43,47–49]

$$\Gamma^{\pm}_{\lambda\lambda'\lambda''} = \frac{\hbar\pi}{8N}\begin{Bmatrix} 2(f_{\lambda'} - f_{\lambda''}) \\ f_{\lambda'} + f_{\lambda''} + 1 \end{Bmatrix} \frac{\delta(\omega_\lambda \pm \omega_{\lambda'} - \omega_{\lambda''})}{\omega_\lambda \omega_{\lambda'} \omega_{\lambda''}} |V^{\pm}_{\lambda\lambda'\lambda''}|^2 \tag{3}$$

and

$$V^{\pm}_{\lambda\lambda'\lambda''} = \sum_{i\in u.c.}\sum_{j,k}\sum_{\alpha\beta\gamma} \frac{e^{\alpha}_{\lambda}(i) e^{\beta}_{p',\pm q'}(j) e^{\gamma}_{p'',-q''}(k)}{\sqrt{M_i M_j M_k}} \Phi^{\alpha\beta\gamma}_{ijk}, \tag{4}$$

where the top (bottom) row in the curly brackets corresponds to the plus (minus) sign of $\Gamma^{\pm}_{\lambda\lambda'\lambda''}$, which represent three-phonon absorption (two phonons merging into one phonon) and emission (one phonon splitting into two) processes. The scattering matrix elements $V^{\pm}_{\lambda\lambda'\lambda''}$ can be evaluated with the normalized eigenvectors $e_{p,q}$ of the three phonons involved and the anharmonic IFCs $\Phi^{\alpha\beta\gamma}_{ijk}$ [43,49]. The contribution of harmonic phonon frequencies to the anharmonic scattering rates can be represented by the three-phonon scattering phase space $W^{\pm}$ (plus and minus signs correspond to absorption and emission processes). It is defined as the sum of frequency-containing factors in the expression of three-phonon transition probabilities [Eq. (3)] and is written as [34]

$$W^{\pm}_{\lambda} = \frac{1}{2N}\sum_{\lambda' p''}\begin{Bmatrix} 2(f_{\lambda'} - f_{\lambda''}) \\ f_{\lambda'} + f_{\lambda''} + 1 \end{Bmatrix} \frac{\delta(\omega_\lambda \pm \omega_{\lambda'} - \omega_{\lambda''})}{\omega_\lambda \omega_{\lambda'} \omega_{\lambda''}}. \tag{5}$$

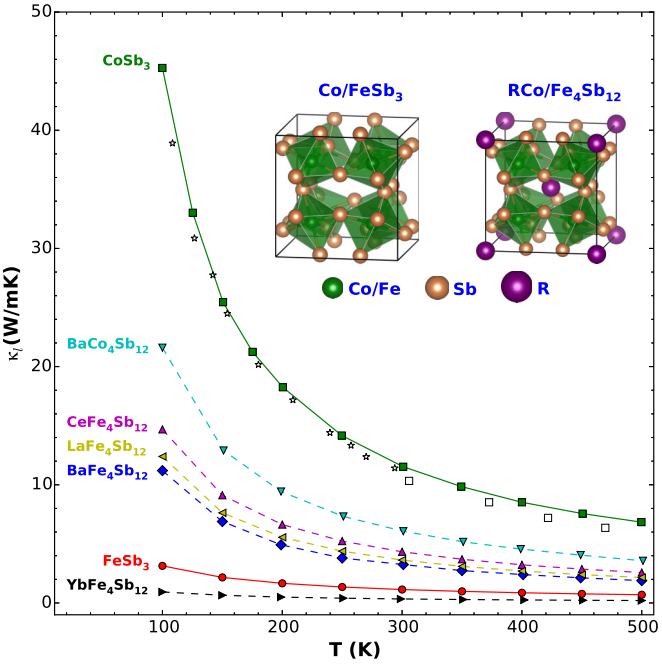

FIG. 1. Calculated temperature dependence of κ_l (in W/mK) of unfilled skutterudites ($FeSb_3$, $CoSb_3$ [50]) and several fully filled skutterudites ($LaFe_4Sb_{12}$, $CeFe_4Sb_{12}$, $YbFe_4Sb_{12}$ [34], $BaFe_4Sb_{12}$ [34], and $BaCo_4Sb_{12}$ [33]). The experimental κ_l for $CoSb_3$ (open symbols) are taken from Morelli *et al.* [51] (stars) and Caillat *et al.* [12] (squares). The inset shows crystal structures of unfilled and fully filled skutterudites.

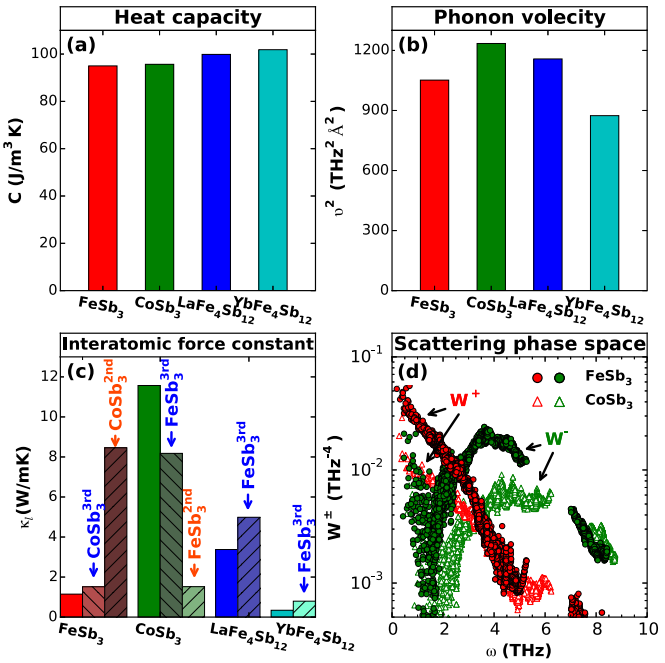

FIG. 2. Analysis of key factors that may affect κ_l for $FeSb_3$, $CoSb_3$, and the filled skutterudites of La/$YbFe_4Sb_{12}$: (a) heat capacity, (b) phonon velocity, (c) interatomic force constant, and (d) scattering phase space. In (b) the phonon velocity is calculated by averaging the group velocities of the long-wavelength (both transverse and longitudinal) acoustic phonons along different phonon momentum directions. In (c) the notation of $M^{n\text{th}}$ represents that the nth-order IFCs of the compound M is used to replace the original IFCs when calculating the room-temperature κ_l.

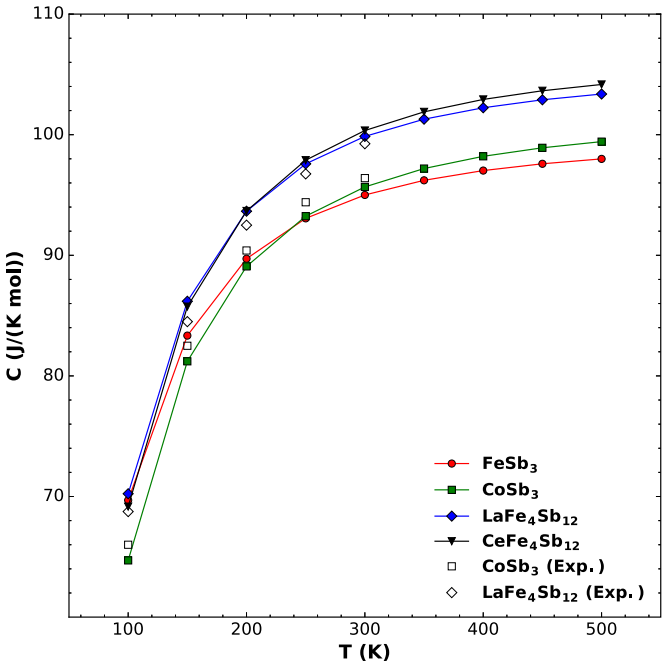

FIG. 3. Calculated heat capacity as a function of temperature for $FeSb_3$, $CoSb_3$, $LaFe_4Sb_{12}$, and $CeFe_4Sb_{12}$. The available experimental data for $CoSb_3$ [40] and $LaFe_4Sb_{12}$ [9] are shown for comparison. The agreement between our calculation and the experiments is good.

III. RESULTS AND DISCUSSION

Figure 1 shows calculated κ_l as a function of temperature for unfilled $FeSb_3$ and $CoSb_3$ [50], as well as the fully filled skutterudites of $LaFe_4Sb_{12}$, $CeFe_4Sb_{12}$, $YbFe_4Sb_{12}$ [34], $BaFe_4Sb_{12}$ [34], and $BaCo_3Sb_{12}$ [33]. The excellent agreement between theoretical results for $CoSb_3$ and available experimental data [12,51] strongly indicates the validity of our calculations. Surprisingly, we find that $FeSb_3$ exhibits a quite low κ_l of 1.14 W/mK at 300 K, about one order of magnitude lower than 11.6 W/mK of $CoSb_3$. In the whole temperature range κ_l of $FeSb_3$ is apparently much lower than the values of most of the filled skutterudites (by more than two-thirds). The only exception is $YbFe_4Sb_{12}$, which has the lowest theoretical κ_l among reported filled skutterudites [34].

We next elucidate the reason why $FeSb_3$ has such an ultralow κ_l. The physical factors that may affect κ_l [see Eq. (1)] include heat capacity C_λ, phonon velocity υ_λ, and phonon lifetime τ_λ of each phonon mode λ. Figures 2(a) and 2(b) show the calculated room-temperature heat capacity and the averaged group velocity over the long-wavelength acoustic phonons contributing predominately to heat carrying, respectively. The difference in the heat capacities of $FeSb_3$ and $CoSb_3$ is negligibly small (less than 0.7%), and their values are ∼7% lower than those of La/$YbFe_4Sb_{12}$. This is almost exactly as expected from the Dulong-Petit law, in accordance with experiments (see Fig. 3). The square of averaged phonon velocity for $FeSb_3$ is about 17% and 10% lower than that of $CoSb_3$ and $LaFe_4Sb_{12}$, respectively. This originates from the substantially reduced frequencies and velocities of the acoustic phonons in $FeSb_3$ (see below). However, the influences of these two factors are far from enough to explain the above large discrepancies in κ_l. Therefore it must be the phonon lifetime that plays a central role in reducing κ_l of $FeSb_3$.

The intrinsic phonon lifetimes of crystalline materials are primarily dominated by the three-phonon anharmonic scattering processes. Figure 4 shows the calculated anharmonic scattering rates at 300 K. As seen, the scattering rates of $FeSb_3$ are nearly one order of magnitude larger than those of $CoSb_3$ in the low- and intermediate-frequency regions (below 5 THz). Clearly, at most of frequencies the scattering rates of $FeSb_3$ are much higher than those of $LaFe_4Sb_{12}$, although lower than those of $YbFe_4Sb_{12}$. Therefore the observed differences in the anharmonic scattering processes that limit phonon lifetimes indeed account for the discrepancies in κ_l. Note that the anharmonic scattering rates of $FeSb_3$ are remarkably enhanced in a wide intermediate frequency range between ∼1 and 5 THz. The behavior is similar to those in La/$YbFe_4Sb_{12}$ and other filled skutterudites [33,34]. This affects contributions of phonon modes to κ_l, as indicated by the cumulative plot of κ_l (κ_l^c) that represents the fraction of heat carried by the phonons with lower frequencies than ω (inset of Fig. 4). The higher anharmonic scattering rates correspond to the smaller lifetimes and thus the smaller contributions of the phonons to κ_l. While, for $CoSb_3$, κ_l^c increase rapidly with ω and the phonons below 2 THz have already contributed to ∼80% of κ_l, κ_l^c of $FeSb_3$ show a much slower increase, and the phonons below 2 THz contribute to only ∼50% of κ_l. The behavior of κ_l^c of $FeSb_3$ resembles those of filled skutterudites, especially $YbFe_4Sb_{12}$.

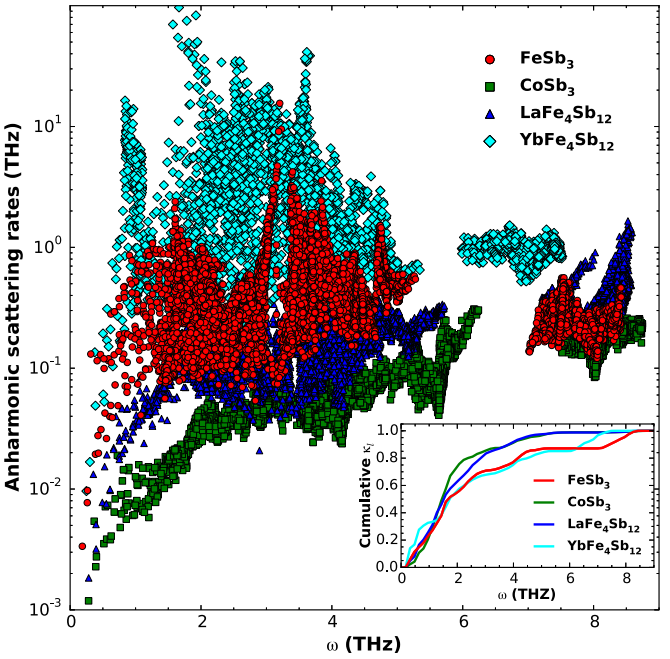

FIG. 4. Calculated anharmonic scattering rates of $FeSb_3$ (red circles), $CoSb_3$ (green squares), $LaFe_4Sb_{12}$ (blue triangles), and $YbFe_4Sb_{12}$ (cyan diamonds) at 300 K. The normalized cumulative κ_l as a function of ω is shown in the inset.

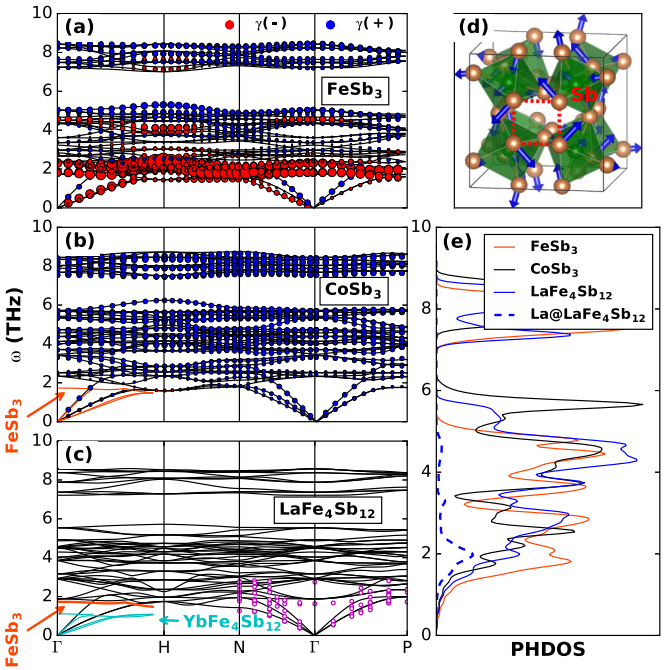

FIG. 5. (a)–(c) Calculated phonon dispersion curves of $FeSb_3$, $CoSb_3$ and $LaFe_4Sb_{12}$. The size of circle represents the magnitude of Grüneisen parameter γ for each mode; positive γ is shown in blue, negative is in red. In (b) and (c) some phonon branches taken from $FeSb_3$ (in orange) and $YbFe_4Sb_{12}$ (in cyan) are shown for comparison. For $LaFe_4Sb_{12}$ in (c), the available experimental data from inelastic neutral scattering measurements [52] are shown (with magenta circles) for comparison. (d) Eigenvector of the lowest optical mode at the Γ point for $FeSb_3$. The Sb_4 ring is indicated with red dashed lines. (e) The (projected) phonon density of states (PHDOS).

We note that Möchel and coworkers found evidence for lattice softening in the latter compound [40].

We further investigate the roles of harmonic and third-order anharmonic IFCs in enhancing three-phonon anharmonic scattering processes and reducing κ_l in $FeSb_3$. In particular we perform calculations of κ_l by deliberately interchanging the harmonic/anharmonic IFCs between two different compounds, as shown in Fig. 2(c). For $FeSb_3$, when replacing the anharmonic IFCs with the ones from $CoSb_3$ and keeping the other quantities unchanged, we find that κ_l increases by ∼30%, whereas κ_l of $CoSb_3$ decreases by ∼30% when using the anharmonic IFCs from $FeSb_3$. The anharmonic scattering rates are generally proportional to the square of the anharmonic IFCs [Eqs. (3) and (4)]. The result means the anharmonic IFCs of $FeSb_3$ are larger than those of $CoSb_3$, corresponding to the higher scattering rates in $FeSb_3$ but far from enough to account for its one order lower κ_l. For the filled skutterudites of $LaFe_4Sb_{12}$ and $YbFe_4Sb_{12}$, when using the anharmonic IFCs from $FeSb_3$, the resulting κ_l show ∼50% and ∼130% increases, respectively. This indicates the anharmonic IFCs of $FeSb_3$ are smaller, corresponding to the lower scattering rates, which conflicts with the smaller κ_l of $FeSb_3$ than that of $LaFe_4Sb_{12}$. When we interchange the harmonic IFCs between $FeSb_3$ and $CoSb_3$, we find κ_l of $FeSb_3$ increases by about 8 times, and κ_l of $CoSb_3$ decreases by almost the same amount. The changes agree well with the discrepancy in κ_l between $FeSb_3$ and $CoSb_3$. From these results, we can conclude that the main factor responsible for the enhanced anharmonic scattering in $FeSb_3$ is the harmonic IFCs, rather than the third-order anharmonic IFCs.

The specific way the harmonic IFCs affect the anharmonic scattering processes is through phonon frequencies and eigenvectors [Eqs. (3) and (4)]. The phonon eigenvectors contribute to the three-phonon scattering matrix elements. Usually, for the same class of materials, the changes in eigenvectors with the varied harmonic IFCs are not as large as the changes in frequencies. It is thus reasonable to assume the scattering matrix elements do not change substantially here. The action of phonon frequencies on the anharmonic scattering is embodied by the three-phonon scattering phase space $W^{\pm}$ [see Eq. (5)], which depicts the available three-phonon scattering channels among all modes. It consists of two components corresponding to absorption (W^+, two phonons merging into one) and emission (W^-, one phonon splitting into two) processes. As shown in Fig. 2(d), W^+ of $FeSb_3$ are distinctly several times larger than those of $CoSb_3$ in the low-frequency (<3.5 THz) region, and W^- of $FeSb_3$ show much larger values in the wide-frequency region below 5 THz as well. The origin of the significantly enhanced $W^{\pm}$ of $FeSb_3$ lies in its distinct phonon spectrum. Compared with that of $CoSb_3$ [Fig. 5(b)], the phonon spectrum of $FeSb_3$ [Fig. 5(a)] shows an overall suppression in frequency. As revealed in Ref. [33], the depressed phonon spectrum can lead to significantly increased W^{+-}. Particularly, $FeSb_3$ exhibits a clear softening of the lowest optical branch (down to below 2 THz). This optical

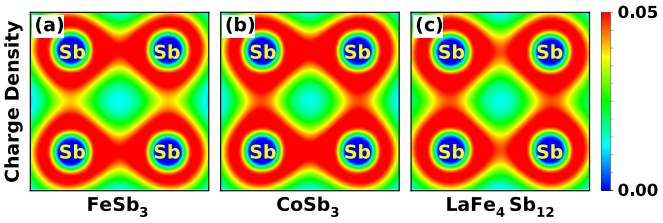

FIG. 6. Contour plot in the (100) plane of charge density on the Sb_4 ring [see Fig. 5(d)] in (a) $FeSb_3$, (b) $CoSb_3$, and (c) $LaFe_4Sb_{12}$. The contour range is from 0 (blue) to 0.05 (red) electron/Å^3.

branch is even lower in frequency than the La-derived rattling mode in $LaFe_4Sb_{12}$ [Fig. 5(c)] and is not far from the extremely low frequency Yb-derived mode in $YbFe_4Sb_{12}$ [cyan curve in Fig. 5(c)]. Actually, it is not only the lowest optical branch but several adjacent upper optical branches that show lowering in frequency in $FeSb_3$. This is unambiguously reflected by a sharp phonon density of states peak appearing around 2 THz [Fig. 5(e)]. It is located in a region similar to that of the La-derived rattling modes in $LaFe_4Sb_{12}$ [blue dashed line in Fig. 5(e)]. The low-lying optical phonons overlap more with the acoustic branches, appreciably increasing the phase space $W^{\pm}$ for three-phonon scattering processes [Fig. 2(d)]. This significantly reduces phonon lifetimes, which is the main root cause for the ultralow κ_l of $FeSb_3$.

Figure 5(d) shows the vibration pattern of the lowest optical phonon mode of $FeSb_3$. It involves torsion of the Sb_4 ring, a typical quasimolecular motif in skutterudites. The lowering in frequency of this optical mode in $FeSb_3$ originates from the weaker Sb-Sb bonds of the Sb_4 ring, as demonstrated by the charge-density plot in Fig. 6. Clearly, the electrons in the Sb_4 ring of $FeSb_3$ are less localized than the case of $CoSb_3$. This indicates the rather weaker Sb-Sb bonds in $FeSb_3$, as expected from its electron-deficient nature. This is consistent with the fact that Young's modulus of $FeSb_3$ is smaller than that of $CoSb_3$ [40,41]. As a result, the phonon modes that are mainly dominated by Sb atoms (below 6 THz) show general softening in $FeSb_3$ [Fig. 5(e)]. The softening also occurs in the acoustic phonons, especially the transverse modes [Fig. 5(b)], which leads to the moderately reduced averaged phonon velocity of $FeSb_3$ in Fig. 2(b). In addition to the phonon softening, the weaker Sb-Sb bonds in $FeSb_3$ result in abnormal Grüneisen parameters γ of phonons [Fig. 5(a)]. For the low-lying optical branches and the transverse acoustic phonons, the values of γ are negative (in red) and quite large in magnitude. Such phonon modes with a large magnitude γ in principle facilitate high lattice anharmonicity [53] and thus low κ_l. The negative sign of γ for the low-lying optical branches implies that they will be further softened under contraction. This is expected to cause more overlapping with acoustic phonons, more enhanced $W^{\pm}$, and thus even lower κ_l at high pressures.

For the filled skutterudites, the electrons of the filler transfer to the host framework following the Zintl behavior [54–56]. Specifically, the electropositive fillers donate charge to the more covalent transition element, the Sb backbone. These electrons are primarily distributed on the Sb_4 ring, which considerably strengthens the Sb-Sb covalent bonds, as indicated in Fig. 6(c) for the $LaFe_4Sb_{12}$ case. This is consistent with the band structure of skutterudites, which shows a light Sb-derived band at the top of the valence bands [57]. This may also explain why filled Fe-based skutterudites are easier to form than $FeSb_3$ usually stabilized in films [37,39,40]. If one considers only the fact that the strengthened Sb-Sb bonds after La filling lift the Sb-derived optical branches in $LaFe_4Sb_{12}$, an increase in κ_l is expected. In fact, the La filler-derived rattling modes play the role of remarkably enhancing $W^{\pm}$. As a result, κ_l of $LaFe_4Sb_{12}$ is still much lower than that of $CoSb_3$ and only about three times larger than that of $FeSb_3$. For the case of $YbFe_4Sb_{12}$, the Yb-derived even lower frequency and rather flat optical phonon branches increase $W^{\pm}$ more significantly, resulting in the more reduced κ_l [34]. Note that flat optical branches generally have large phase space for anharmonic scattering but by themselves do not carry substantial heat regardless.

IV. CONCLUSIONS

To summarize, we reported a discovery of ultralow κ_l in pure skutterudite $FeSb_3$ with no filler by using first-principles Boltzmann-Peierls transport simulations. The calculated κ_l is only 1.14 W/mK at room temperature, one order of magnitude lower than that of $CoSb_3$. It is even lower than κ_l of most fully filled skutterudites. This is in contrast to the widely used approach where filling is used to reduce κ_l in skutterudites. The origin of the ultralow κ_l is attributed to the overall softening of phonon spectrum, especially the optical phonons

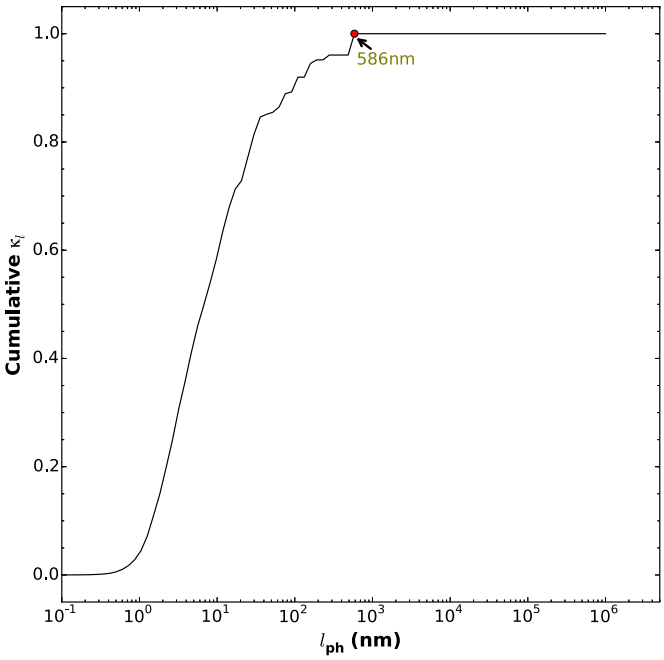

FIG. 7. The normalized cumulative κ_l of $FeSb_3$ as a function of the phonon mean free path l_{ph} at 300 K. The maximum phonon l_{ph} among all the modes that conduct heat efficiently, which corresponds to the onset point of the cumulative κ_l approaching 1.0, is indicated.

with a remarkable decrease in frequency associated with the weaker Sb-Sb bonds in $FeSb_3$ owing to its electron-deficient nature. These low-frequency optical phonons play the role of the rattling modes in filled skutterudites. Particularly, they overlap more with the heat-carrying acoustic phonons and increase the phase space of three-phonon anharmonic scattering processes, resulting in significantly reduced phonon lifetimes and thus ultralow κ_l. Our results offer insight into the still-debated mechanism responsible for the κ_l reduction upon filling in skutterudites and also a routine for lowering κ_l of skutterudite-type thermoelectric materials. Finally, we evaluated the maximum mean free path l_{ph} of phonons that conduct heat efficiently for bulk $FeSb_3$, as shown in Fig. 7. The purpose of such a calculation is to provide a reference for future experimental measurements about at least how thick thin-film samples should be adopted to measure the intrinsic κ_l of the bulk $FeSb_3$ we calculated here. According to our result, the maximum l_{ph} is less than 600 nm. A sample size above this value is needed to safely avoid surface and grain-boundary scatterings. Therefore experimentally synthesized $FeSb_3$ films with a thicknesses of 1.0–1.5 μm [40] may be directly applied to measure the intrinsic κ_l and verify our theoretical prediction.

ACKNOWLEDGMENTS

The authors acknowledge funding support from the Recruitment Program of Global Youth Experts in China and special funds for talent development in Jilin Province. Part of the calculations was performed at the high-performance computing center of Jilin University and on TianHe-1 (A) of the National Supercomputer Center in Tianjin. The work of D.J.S. is supported by S3TEC, an Energy Frontier Research Center funded by the Department of Energy, Office of Science, Basic Energy Sciences under Award No. DE-SC0001299/DE-FG02-09ER46577.

[1] D. T. Morelli and G. P. Meisner, J. Appl. Phys. **77**, 3777 (1995).
[2] B. C. Sales, D. Mandrus, and R. K. Williams, Science **272**, 1325 (1996).
[3] G. S. Nolas, D. T. Morelli, and T. M. Tritt, Annu. Rev. Mater. Sci. **29**, 89 (1999).
[4] X. Shi, J. Yang, J. R. Salvador, M. Chi, J. Y. Cho, H. Wang, S. Bai, J. Yang, W. Zhang, and L. Chen, J. Am. Chem. Soc. **133**, 7837 (2011).
[5] D. J. Singh and I. I. Mazin, Phys. Rev. B **56**, R1650 (1997).
[6] W. Zhang, X. Shi, Z. G. Mei, Y. Xu, L. D. Chen, J. Yang, and G. P. Meisner, Appl. Phys. Lett. **89**, 112105 (2006).
[7] D. T. Morelli, G. P. Meisner, B. Chen, S. Hu, and C. Uher, Phys. Rev. B **56**, 7376 (1997).
[8] G. Rogl, A. Grytsiv, E. Bauer, P. Rogl, and M. Zehetbauer, Intermetallics **18**, 57 (2010).
[9] W. Schnelle, A. Leithe-Jasper, H. Rosner, R. Cardoso-Gil, R. Gumeniuk, D. Trots, J. A. Mydosh, and Y. Grin, Phys. Rev. B **77**, 094421 (2008).
[10] H. Li, X. Tang, Q. Zhang, and C. Uher, Appl. Phys. Lett. **94**, 102114 (2009).
[11] J. S. Dyck, W. Chen, C. Uher, L. Chen, X. Tang, and T. Hirai, J. Appl. Phys. **91**, 3698 (2002).
[12] T. Caillat, A. Borshchevsky, and J. Fleurial, J. Appl. Phys. **80**, 4442 (1996).
[13] J. Yang and T. Caillat, MRS Bull. **31**, 224 (2006).
[14] J. Yang, P. Qiu, R. Liu, L. Xi, S. Zheng, W. Zhang, L. Chen, D. J. Singh, and J. Yang, Phys. Rev. B **84**, 235205 (2011).
[15] G. S. Nolas, M. Kaeser, R. T. Littleton, and T. M. Tritt, Appl. Phys. Lett. **77**, 1855 (2000).
[16] L. D. Chen, T. Kawahara, X. F. Tang, T. Goto, T. Hirai, J. S. Dyck, W. Chen, and C. Uher, J. Appl. Phys. **90**, 1864 (2001).
[17] G. A. Lamberton, S. Bhattacharya, R. T. Littleton, M. A. Kaeser, R. H. Tedstrom, T. M. Tritt, J. Yang, and G. S. Nolas, Appl. Phys. Lett. **80**, 598 (2002).
[18] L. Zhang, A. Grytsiv, P. Rogl, E. Bauer, and M. Zehetbauer, J. Phys. D **42**, 225405 (2009).
[19] G. Rogl, A. Grytsiv, P. Rogl, N. Peranio, E. Bauer, M. Zehetbauer, and O. Eibl, Acta Mater. **63**, 30 (2014).
[20] J. Yang, L. Xi, W. Qiu, L. Wu, X. Shi, L. Chen, J. Yang, W. Zhang, C. Uher, and D. J. Singh, npj Comput. Mater. **2**, 15015 (2016).
[21] G. A. Slack, in *CRC Handbook of Thermoelectrics*, edited by D. M. Rowe (CRC Press, Boca Raton, FL, 1995), p. 402.
[22] X. Y. Zhao, X. Shi, L. D. Chen, W. Q. Zhang, W. B. Zhang, and Y. Z. Pei, J. Appl. Phys. **99**, 053711 (2006).
[23] Y. Z. Pei, L. D. Chen, W. Zhang, X. Shi, S. Q. Bai, X. Y. Zhao, Z. G. Mei, and X. Y. Li, Appl. Phys. Lett. **89**, 221107 (2006).
[24] P. F. Qiu, J. Yang, R. H. Liu, X. Shi, X. Y. Huang, G. J. Snyder, W. Zhang, and L. D. Chen, J. Appl. Phys. **109**, 063713 (2011).
[25] G. A. Slack and V. G. Tsoukala, J. Appl. Phys. **76**, 1665 (1994).
[26] V. Keppens, D. Mandrus, B. Sales, B. Chakoumakos, P. Dai, R. Coldea, M. Maple, D. Gajewski, E. Freeman, and S. Bennington, Nature (London) **395**, 876 (1998).
[27] R. P. Hermann, R. Jin, W. Schweika, F. Grandjean, D. Mandrus, B. C. Sales, and G. J. Long, Phys. Rev. Lett. **90**, 135505 (2003).
[28] H.-C. Wille, R. P. Hermann, I. Sergueev, O. Leupold, P. van der Linden, B. C. Sales, F. Grandjean, G. J. Long, R. Rüffer, and Y. V. Shvyd'ko, Phys. Rev. B **76**, 140301 (2007).
[29] M. M. Koza, M. R. Johnson, R. Viennois, H. Mutka, L. Girard, and D. Ravot, Nat. Mater. **7**, 805 (2008).
[30] J. L. Feldman, D. J. Singh, I. I. Mazin, D. Mandrus, and B. C. Sales, Phys. Rev. B **61**, R9209 (2000).
[31] A. Yamakage and Y. Kuramoto, J. Phys. Soc. Jpn. **78**, 064602 (2009).
[32] N. Bernstein, J. L. Feldman, and D. J. Singh, Phys. Rev. B **81**, 134301 (2010).
[33] W. Li and N. Mingo, Phys. Rev. B **89**, 184304 (2014).
[34] W. Li and N. Mingo, Phys. Rev. B **91**, 144304 (2015).
[35] B. C. Sales, D. Mandrus, B. C. Chakoumakos, V. Keppens, and J. R. Thompson, Phys. Rev. B **56**, 15081 (1997).

[36] C. H. Lee, I. Hase, H. Sugawara, H. Yoshizawa, and H. Sato, J. Phys. Soc. Jpn. **75**, 123602 (2006).
[37] M. V. Daniel, L. Hammerschmidt, C. Schmidt, F. Timmermann, J. Franke, N. Jöhrmann, M. Hietschold, D. C. Johnson, B. Paulus, and M. Albrecht, Phys. Rev. B **91**, 085410 (2015).
[38] G. Xing, X. Fan, W. Zheng, Y. Ma, H. Shi, and D. J. Singh, Sci. Rep. **5**, 10782 (2015).
[39] M. D. Hornbostel, E. J. Hyer, J. Thiel, and D. C. Johnson, J. Am. Chem. Soc. **119**, 2665 (1997).
[40] A. Möchel, I. Sergueev, N. Nguyen, G. J. Long, F. Grandjean, D. C. Johnson, and R. P. Hermann, Phys. Rev. B **84**, 064302 (2011).
[41] M. Råsander, L. Bergqvist, and A. Delin, Phys. Rev. B **91**, 014303 (2015).
[42] S. Lemal, N. Nguyen, J. de Boor, P. Ghosez, J. Varignon, B. Klobes, R. P. Hermann, and M. J. Verstraete, Phys. Rev. B **92**, 205204 (2015).
[43] W. Li, J. Carrete, N. A. Katcho, and N. Mingo, Comput. Phys. **185**, 1747 (2014).
[44] P. E. Blöchl, Phys. Rev. B **50**, 17953 (1994).
[45] G. Kresse and J. Furthmüller, Phys. Rev. B **54**, 11169 (1996).
[46] A. Togo, F. Oba, and I. Tanaka, Phys. Rev. B **78**, 134106 (2008).
[47] D. A. Broido, M. Malorny, G. Birner, N. Mingo, and D. A. Stewart, Appl. Phys. Lett. **91**, 231922 (2007).
[48] A. Ward, D. A. Broido, D. A. Stewart, and G. Deinzer, Phys. Rev. B **80**, 125203 (2009).
[49] W. Li, L. Lindsay, D. A. Broido, D. A. Stewart, and N. Mingo, Phys. Rev. B **86**, 174307 (2012).
[50] W. Li and N. Mingo, Phys. Rev. B **90**, 094302 (2014).
[51] D. T. Morelli, T. Caillat, J.-P. Fleurial, A. Borshchevsky, J. Vandersande, B. Chen, and C. Uher, Phys. Rev. B **51**, 9622 (1995).
[52] M. M. Koza, M. Boehm, E. Sischka, W. Schnelle, H. Mutka, and A. Leithe-Jasper, Phys. Rev. B **91**, 014305 (2015).
[53] J. S. Dugdale and D. K. C. MacDonald, Phys. Rev. **98**, 1751 (1955).
[54] D. Braun and W. Jeitschko, J. Less Common Metals **72**, 147 (1980).
[55] G. A. Papoian and R. Hoffmann, Angew. Chem. Int. Ed. **39**, 2408 (2000).
[56] H. Luo, J. W. Krizan, L. Muechler, N. Haldolaarachchige, T. Klimczuk, W. Xie, M. K. Fuccillo, C. Felser, and R. J. Cava, Nat. Commun. **6**, 6489 (2015).
[57] D. J. Singh and W. E. Pickett, Phys. Rev. B **50**, 11235 (1994).